

Explaining the paradoxical diversity of ultrafast laser-induced demagnetization

B. Koopmans¹*, G. Malinowski¹, F. Dalla Longa¹, D. Steiauf², M. Fähnle², T. Roth³, M. Cinchetti³ and M. Aeschlimann³

Pulsed-laser-induced quenching of ferromagnetic order has intrigued researchers since pioneering works in the 1990s. It was reported that demagnetization in gadolinium proceeds within 100 ps, but three orders of magnitude faster in ferromagnetic transition metals such as nickel. Here we show that a model based on electron-phonon-mediated spin-flip scattering explains both timescales on equal footing. Our interpretation is supported by *ab initio* estimates of the spin-flip scattering probability, and experimental fluence dependencies are shown to agree perfectly with predictions. A phase diagram is constructed in which two classes of laser-induced magnetization dynamics can be distinguished, where the ratio of the Curie temperature to the atomic magnetic moment turns out to have a crucial role. We conclude that the ultrafast magnetization dynamics can be well described disregarding highly excited electronic states, merely considering the thermalized electron system.

For more than two decades, researchers have been attracted to the question: what happens in a ferromagnet after suddenly exciting it by a short laser pulse, rapidly heating up the electron gas? Identifying the channel for transfer of angular momentum accompanying the successive ultrafast loss of magnetic order has been the key issue in the field. In the early 1990s, Vaterlaus and co-workers carried out time- and spin-resolved photoemission (TSPE) experiments on gadolinium, yielding a rough estimate of the demagnetization time, $\tau_M \sim 100 \pm 80$ ps (ref. 1). This value was soon thereafter reproduced by theoretical estimates of spin-lattice relaxation². In view of the above, new results in 1996 by Beaurepaire *et al.* exploiting time-resolved magneto-optical Kerr effect (TRMOKE) studies on nickel thin films came as quite a surprise³. It was found that demagnetization after sub-100 fs pulsed-laser excitation proceeds well within a picosecond. By now, this result has been confirmed for all elementary ferromagnetic transition metals (Co, Ni, Fe) and several alloys thereof (see ref. 4 and references therein). Important further confirmation came by a wide range of alternative techniques, such as TSPE (ref. 5), time-resolved studies of the exchange-splitting⁶, as well as X-ray magnetic circular dichroism⁷ (XMCD).

Despite this experimental progress, it turned out to be difficult to identify the underlying microscopic mechanism, let alone explain the contrasting timescales for Ni and Co versus that of Gd on equal footing. Beaurepaire *et al.* introduced a phenomenological three-temperature model (3TM), describing the interaction between the electron, spin and lattice sub-systems³. Pure energy transfer from the optically excited hot electrons to the lattice takes typically 0.5–1 ps, whereas demagnetization is essentially described by an angular momentum transfer from electrons or lattice to the spin system (Fig. 1a,c). However, the 3TM does not take into account considerations regarding the transfer of angular momentum. Zhang and Hübner proposed a channel for ultrafast transfer between spin- and orbital momenta, however without including the lattice degree of freedom⁸. Dissipation of angular momentum was explicitly addressed by Koopmans *et al.*, who introduced a microscopic

model based on the Elliott–Yafet type of scattering, described by a probability a_{sf} that an electron flips its spin on emission or absorption of a phonon⁹ (Fig. 1e). More recently, an atomistic approach to the Landau–Lifshitz–Gilbert equation was shown to lead to similar dynamics^{10,11}.

In agreement with the Elliott–Yafet model, Stamm *et al.* showed by XMCD on Ni thin films that a rapid transfer between orbital and spin moment is not of relevance, leaving only dissipation of angular momentum into the lattice as a viable channel⁷. A similar conclusion was drawn by Cinchetti *et al.*¹². New experiments by Melnikov, Bovensiepen and co-workers on gadolinium^{13–17} (Wietstruk *et al.*, submitted) confirmed the relatively slow demagnetization (50–100 ps) originally reported by Vaterlaus, but also identified a partial demagnetization at a much faster timescale (~ 1 ps, schematically represented in Fig. 1b).

Here, we introduce a theoretical framework that successfully explains all phenomena and timescales on equal footing. Although a simple model Hamiltonian⁴ is used, the spin-flip probability a_{sf} deduced is shown to agree well with *ab initio* calculations of the spin-mixing in the elementary ferromagnets. Moreover, we present detailed laser-fluence-dependent studies on Ni and Co, which show a behaviour very similar to the model's predictions. Finally, we show that the two-step demagnetization observed in the experiments on Gd is a natural consequence of our model. More generally, we present a generic view on laser-induced demagnetization, introducing a phase diagram separating two classes of dynamics.

Demagnetization by spin-flip scattering

The starting point of our theoretical analysis is the phenomenological 3TM (ref. 3), in which we implement a microscopic description of the spin dynamics. In the ordinary 3TM, heat capacities and temperatures are assigned to the reservoirs of electron charge (e), spin (s) and lattice/phonons (p), (C_e, T_e), (C_s, T_s) and (C_p, T_p), respectively. Furthermore, coupling constants are defined as g_{es}, g_{sp} and g_{ep} , describing the rate of energy exchange between the participating

¹Department of Applied Physics, Center for NanoMaterials (cNM), Eindhoven University of Technology, PO Box 513, 5600 MB Eindhoven, The Netherlands, ²Max-Planck-Institut für Metallforschung Stuttgart, Heisenbergstraße 3, 70569 Stuttgart, Germany, ³Department of Physics and Research Center OPTIMAS, University of Kaiserslautern, Erwin-Schrödinger-Straße 46, 67663 Kaiserslautern, Germany. *e-mail: B.Koopmans@tue.nl

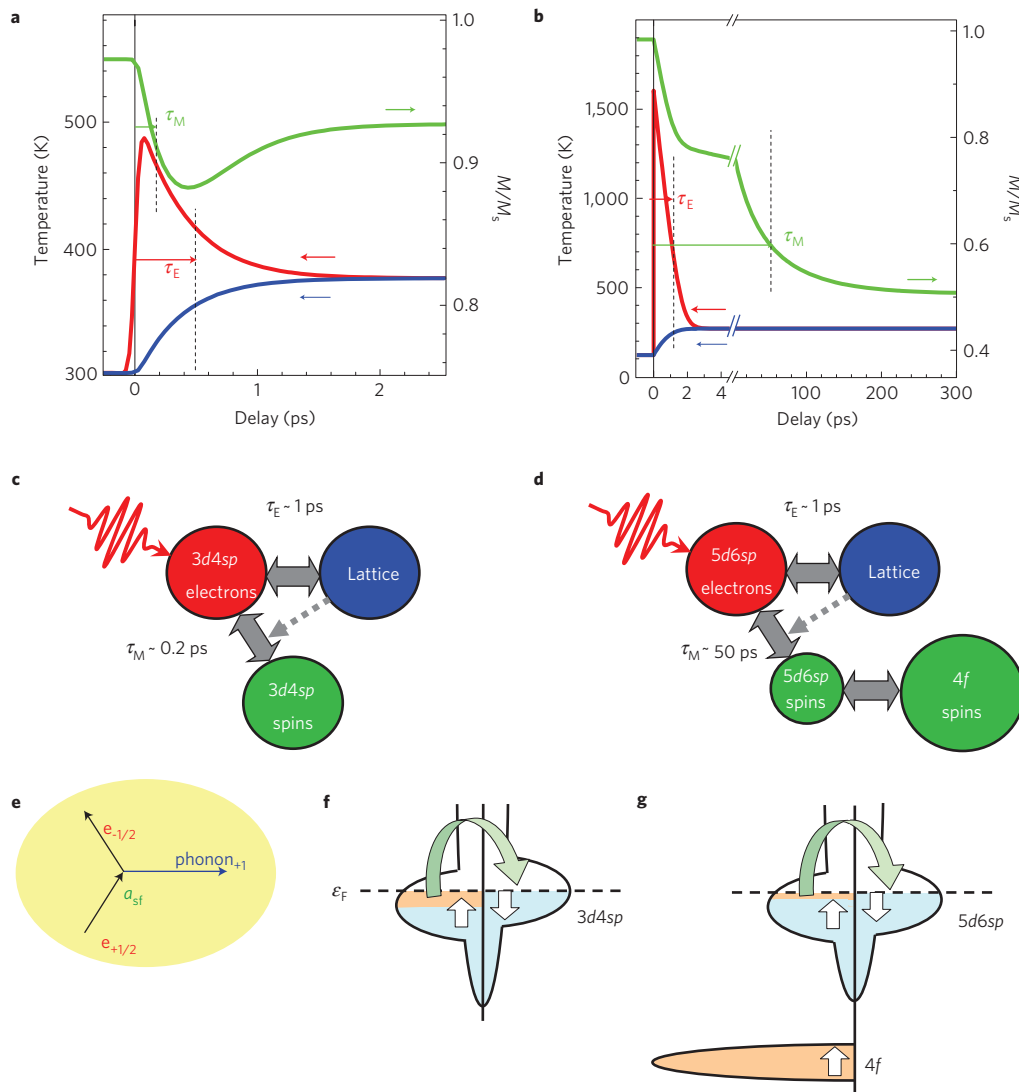


Figure 1 | Schematic representations of laser-induced demagnetization of Ni compared with Gd. **a**, Ultrafast demagnetization $m(t)$ (green), as well as $T_e(t)$ (red) and $T_p(t)$ (blue) profiles, simulating experimental results for Ni. **b**, Similar for the two-step process, as observed for Gd. **c**, 3TM variant as a representative for the present work on 3d transition metals. Energy equilibration is indicated by two-sided arrows; angular momentum flow is controlled by interaction with the lattice (dashed arrow). **d**, Similar for Gd, with the extra 4f system. **e**, Elliott–Yafet spin-flip scattering on emission of a phonon, taking over angular momentum. **f**, Spin-flip scattering in the 3d4sp band of Ni, schematically illustrated in a density of states plot, in which states are filled to the Fermi energy, ϵ_F . The orange shading represents the number of uncompensated spins. **g**, Similar diagram for Gd; scattering is occurring only in the 5d6sp band with small magnetic moment, whereas localized 4f states predominantly contribute to the magnetic moment.

sub-systems. Thus, the overall dynamics is phenomenologically described by a set of three coupled differential equations (for T_e , T_p and T_s). In cases where we want to make a quantitative comparison to experiments, we use an approach for finite film thickness, including non-homogeneous heating and electronic heat diffusion.

In our microscopic implementation of the 3TM, referred to as M3TM, spin relaxation is mediated by Elliott–Yafet-like processes, with a spin-flip probability a_{sf} for electron–phonon momentum scattering events. We derived a compact differential equation for the magnetization dynamics (see the Methods section)

$$\frac{dm}{dt} = Rm \frac{T_p}{T_C} \left(1 - m \coth \left(\frac{mT_C}{T_e} \right) \right) \quad (1)$$

where $m = M/M_s$ (the magnetization relative to its value at zero temperature) and T_C denotes the Curie temperature. The prefactor R (unit s^{-1}) provides a materials-specific scaling factor for the demagnetization rate. Its dependence on relevant magnetic

parameters is given by $R \propto a_{sf} T_C^2 / \mu_{at}$, where μ_{at} is the atomic magnetic moment. Note that conservation and transfer of angular momentum is explicitly taken into account. Whereas it is the excess energy in the electron system that provides the energy for the demagnetization, interaction with the lattice provides a dissipative channel for angular momentum (Fig. 1c,e). We stress that we assume the electronic system to be in full internal equilibrium throughout our calculations; that is, we neglect the finite thermalization time, which typically is ~ 50 – 100 fs.

Equation (1) in combination with the differential equations for T_e and T_p from the 3TM will be used to fit experimental demagnetization transients, and thereby extract a value for a_{sf} . The last parameter is related to the spin-mixing of electronic states near the Fermi level ϵ_F , as we calculated by the *ab initio* density functional electron theory. As a result of the spin–orbit coupling, a single-electron eigenstate ψ_k in a solid is always a mixture of the two spin states $|\uparrow\rangle$ and $|\downarrow\rangle$, for example, a dominant spin-up contribution $a_k|\uparrow\rangle$ and a small spin-down contribution $b_k|\downarrow\rangle$. The spin-mixing

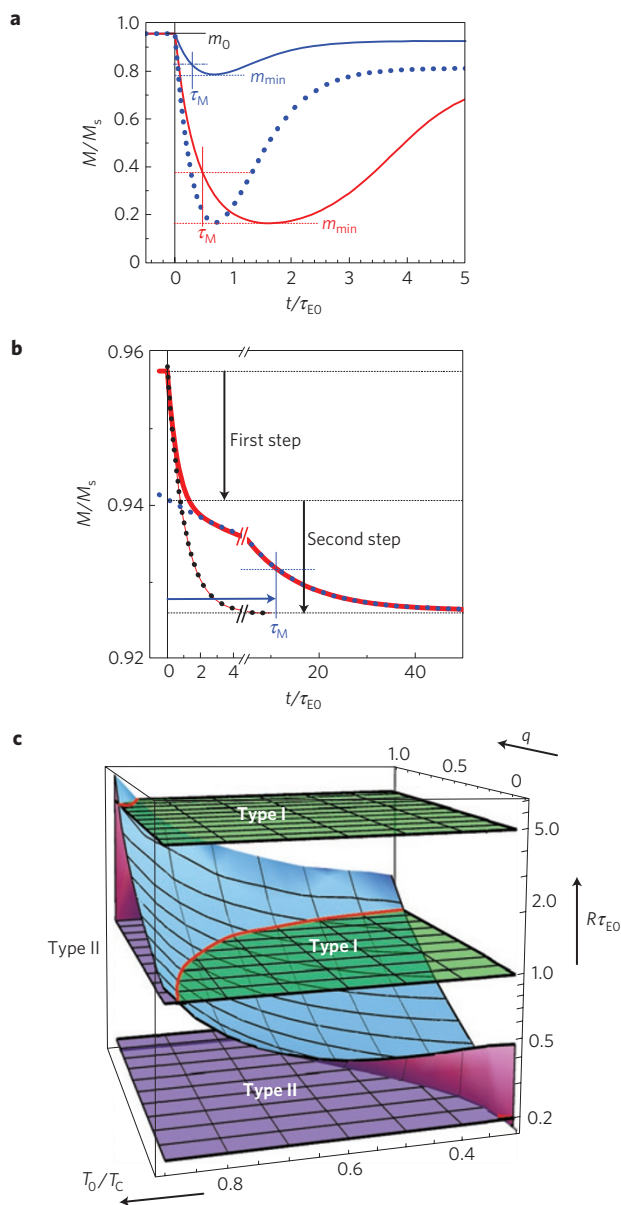


Figure 2 | Type I and type II magnetization dynamics. **a**, Type I dynamics at $T = 0.5 T_C$ for a fictitious material ($C_p = 5\gamma T_C$) with a large spin-flip rate ($R = 5.0\tau_{E0}^{-1}$), leading to single-step demagnetization within the electron–phonon equilibration. Results for demagnetization at low (blue) and high (red) laser fluence are shown ($q = 0.2$ and 0.8 , respectively), as well as a scaled version of the low-fluence result (blue dotted). The time axis is normalized to τ_{E0} , defined as τ_E at $T \approx T_C$. **b**, Two-step demagnetization (type II) as observed for materials with a small value of $R(0.2\tau_{E0}^{-1})$. **c**, Generalized phase diagram, for materials with a certain relative spin-flip rate $R\tau_{E0}$ as a function of fluence q and ambient temperature T_0/T_C (see text). The curved plane (top side blue, bottom side red) separates regions of type I and type II dynamics. The opaque planes represent different materials ($R\tau_{E0} = 5.0, 1.0$ and 0.2 , respectively), where green represents type I behaviour, and purple type II behaviour.

parameter $\langle b^2 \rangle$ of the Elliott–Yafet theory is then defined as

$$\langle b^2 \rangle = \overline{\min(\langle \psi_k | \uparrow \rangle \langle \uparrow | \psi_k \rangle, \langle \psi_k | \downarrow \rangle \langle \downarrow | \psi_k \rangle)} \quad (2)$$

where the bar denotes a suitably defined average over all states involved in the Elliott–Yafet scattering processes^{18,19}.

Classification of ultrafast dynamics

Despite its simplicity, equation (1) predicts a rich variety of features. Figure 2a shows time traces in the limit of large R . In this regime, denoted as type I dynamics, demagnetization completes before electron–phonon equilibration is achieved. At low fluence (blue solid line), one observes a rapid demagnetization, followed by a pronounced recovery of M at the electron–phonon equilibration timescale τ_E . Carrying out experiments at a fixed fluence as a function of ambient temperature T_0 , a critical slowing down of the demagnetization when approaching T_C is observed (not shown, see also ref. 9). Fixing T_0 , but repeating the experiment at a higher laser fluence, the demagnetization is stronger but proceeds slower (Fig. 2a, red line; the blue dotted line represents the low-fluence data scaled to the minimum of the high fluence). Similarly, the recovery slows down significantly^{10,20}.

The magnetization dynamics changes markedly in the limit of small R , leading to type II dynamics. In this regime, the demagnetization efficiency is insufficient to establish a full thermal equilibrium of the spin system during electron–phonon equilibration. As at higher electron temperature the demagnetization is more efficient, it means that after an initial rapid decay (black dotted line in Fig. 2b), around $t \approx \tau_E$ a transition occurs to a lower demagnetization rate. Moreover, right after laser heating, the spin system seeks to equilibrate to the temperature of the heated electron gas, whereas after electron–phonon equilibration it continues to equilibrate towards a more moderate temperature. For both mechanisms, the timescale of the initial drop in magnetization is equal to the non-magnetic τ_E , during which the demagnetization proceeds faster (blue dotted line).

Applying our theory to different materials measured at equal ambient temperature T_0 , the explicit expression of the prefactor in equation (1), RmT_p/T_C , shows that the ratio T_C/μ_{at} has a decisive role, which we will refer to as the figure of merit for the demagnetization time. For materials with similar a_{sf} , a smaller figure of merit will cause a slower demagnetization and thereby the tendency to show two-step, type II dynamics. Figure 2c shows a generic phase diagram predicting the type of dynamics for arbitrary laser fluence and ambient temperature T_0 . Rather than plotting as a function of actual laser fluence, the maximum quenching of the magnetization ($q = 1 - m_{min}/m_0$, where m_0 is the normalized magnetization at $T = T_0$) is used. The curved plane separates regions of type I and type II dynamics. Materials with a large figure of merit, leading to a large $R \gg \tau_{E0}^{-1}$ (such as represented by the top plane, $R = 5.0\tau_{E0}^{-1}$, where τ_{E0} is defined as τ_E at $T \approx T_C$), show type I dynamics for all conditions, whereas materials with small $R \ll \tau_{E0}^{-1}$ show type II dynamics (bottom plane, $R = 0.2\tau_{E0}^{-1}$). Materials with an intermediate $R \approx \tau_{E0}^{-1}$ can be driven from type I to type II at large fluences or ambient temperatures close to T_C (for example, middle plane, $R = 1.0\tau_{E0}^{-1}$).

Type I dynamics: Ni and Co

To make contact between our microscopic description of the demagnetization dynamics and experiments on elementary ferromagnetic transition metals, we carried out TRMOKE measurements on Ni and Co thin films, at fluences ranging from small (from ref. 21) to high enough to cause a quenching of most of the magnetization (this work, see the Methods section). All of these experiments were carried out at T_0 equal to room temperature. A typical magnetization trace for Ni at low fluence is shown in Fig. 3a. Following the fitting procedure outlined in the Methods section, we find $a_{sf} = 0.19 \pm 0.03$ at low fluence.

We next discuss measurements on Ni at higher fluences (Fig. 3b). Fitted curves based on our model reproduce the evolution of the time traces as a function of fluence remarkably well. Figure 3d shows a plot of the values of τ_M extracted at each fluence, and compares them to theory. A perfect match is found for

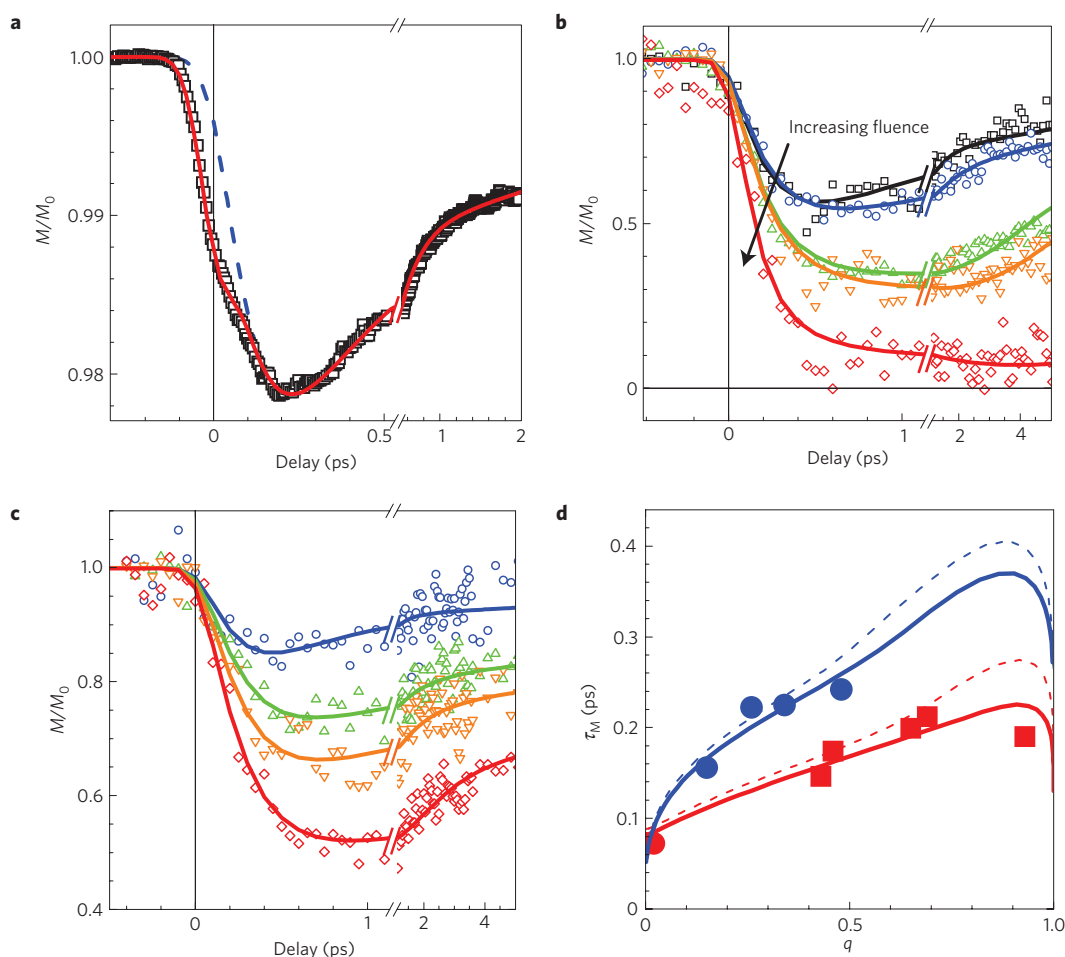


Figure 3 | TRMOKE experiments on Ni and Co for different laser fluences, as compared to results of the M3TM model. **a**, Experimental demagnetization for a Ni (10 nm) thin film in the low-fluence limit (for experimental details, see ref. 21). The red line represents a simulated curve using $a_{sf} = 0.19$; the dashed blue line corresponds to the simulation while excluding an instantaneous peak at zero delay (see the Methods section). **b**, Similar demagnetization curves for a 15 nm film and higher fluences, ranging from 2.2 mJ cm⁻² (black, squares) via intermediate value, (blue circles, green and orange triangles), to 5.0 mJ cm⁻² (red, diamonds) per pulse. Curves are corresponding fits using the demagnetization quenching q and a_{sf} as fitting parameters, while keeping thermodynamic parameters constant. Heat diffusion is included as explained in the Methods section. **c**, Similar data for Co (15 nm). **d**, Demagnetization times τ_M as fitted from $M(t)/M_0$ for Ni (red squares) and Co (blue circles) as a function of q . The drawn lines are model predictions for a 15 nm film, including heat diffusion, and using $a_{sf} = 0.185$ and 0.150 for Ni and Co, respectively. The dashed lines are the prediction for an infinitesimally thin film on a thermally insulating substrate.

$a_{sf} = 0.185 \pm 0.015$, independent of fluence—showing that our theory can predict the trends of the demagnetization dynamics at high fluence once the dynamics at low fluence is known. We stress that if the demagnetization time would have been governed by the electron thermalization, as previously suggested, it should actually speed up rather than slow down at elevated temperature, where thermalization proceeds more rapidly²². The mere fact that at high fluence we observe a fast demagnetization up to 0.5 ps, well after electron thermalization (<100 fs), supports our claim that non-thermal electrons are not of decisive importance for the ultrafast demagnetization.

A similar fluence-dependent study has been carried out for Co (Fig. 3c). As a result of the much higher T_C in comparison with Ni (1,388 K versus 627 K), the maximum demagnetization achieved stays well below that of nickel. It is interesting to note that the ratio of their T_C is almost equal to the ratio of μ_{at} (1.72 μ_B versus 0.62 μ_B), and therefore the figure of merit, T_C/μ_{at} , would be approximately equal for Co and Ni. Indeed, Fig. 3d shows very similar values of τ_M in comparison to Ni. A least-squares fit yields a spin-flip probability $a_{sf} = 0.150 \pm 0.015$, only slightly smaller than for Ni.

Although we obtained a proper match between the experimental data and the model for all fluences and both Ni and Co, the relatively large $a_{sf} \approx 0.1$ –0.2 may seem worrying. It would mean that more than one out of ten momentum scattering events would be accompanied by a spin-flip process. Usually, a_{sf} scales with the nuclear charge Z according to $a_{sf} \propto Z^4$ owing to spin–orbit coupling, resulting in a value of approximately 0.001 for Cu (ref. 23), which has a similar Z as Ni and Co. In earlier publications, we speculated on an increased a_{sf} owing to enhanced spin-mixing near hot spots in the electronic band structure. Such band crossings near the ε_F in aluminium have been demonstrated to result in an enhancement by two orders of magnitude with respect to the Z^4 scaling rule²⁴.

Motivated by the lack of data on spin-mixing for the ferromagnetic transition metals, we carried out *ab initio* calculations for $\langle b^2 \rangle$ of Ni and Co according to equation (2). We averaged over all electronic states near ε_F , sampling the Brillouin zone with a Gaussian smearing function for the occupation numbers, centred at ε_F and using a smearing parameter σ . Results for two extreme cases of σ are summarized in Table 1. We insert on the one hand $\sigma = 25$ meV, which means that the dominant contribution to the

Table 1 | *Ab initio* calculations of the spin-mixing parameter (b^2) for Ni, Co and Gd, using different smearing parameters, corresponding 'thermal' smearing ($\sigma = 25$ meV), and 'optical' smearing ($\sigma = 1.4$ eV).

	$\langle b^2 \rangle$ $\sigma = 25$ meV	$\langle b^2 \rangle$ $\sigma = 1.4$ eV	$p(b^2)$ range*	a_{sf} (exp.) [†]	τ_M (theory) [‡] (ps)	τ_M (exp.) [‡] (ps)
Ni	0.025	0.045	0.03–0.45	0.185 ± 0.015	0.21	0.16
Co	0.011	0.049	0.01–0.50	0.150 ± 0.015	0.34	0.26
Gd	0.06	0.06	0.06–0.60	0.08 ± 0.02	15	40

*The column labelled $p(b^2)$ yields the minimum and maximum values considering both thermal and optical smearing, and assuming $1 < p < 10$.

[†]The column labelled a_{sf} shows the value as fitted from experimental data and using the model discussed throughout this article.

[‡]The final two columns compare the theoretical prediction (theory) and experimentally deduced values (exp.) for τ_M for the specific case of using a fluence that leads to a quenching of the magnetization by 50%. The quoted theoretical value is based on an 'intermediate value' $p = 4$ and $\langle b^2 \rangle$ averaged over $\sigma = 25$ meV and 1.4 eV.

demagnetization arises from thermally excited electrons and holes. On the other hand we use $\sigma = 1.4$ eV, which would mean that all quasiparticles that can be produced by an optical laser pulse at 1.4 eV contribute to the demagnetization. The relationship between spin-mixing and spin-flip probability can be written as $a_{sf} = p\langle b^2 \rangle$, with $p \sim 1$ –10 (see the Methods section). The range of possible values of a_{sf} predicted this way, including both the uncertainty in p and in σ , is indicated in Table 1. We thus find that Ni and Co have quite similar spin-mixing near ε_F . Both values are approximately two orders of magnitude larger compared with Cu owing to regions with increased spin-flip scattering in the band structure ('hot spots'), in line with recent findings for Co (ref. 25). Furthermore, the values for a_{sf} we deduced from our microscopic model and experiments correspond well with the range of *ab initio* predictions—providing further support for the feasibility of our model for ultrafast magnetization dynamics.

Type II dynamics: Gd and other materials

Having established a proper match for Ni and Co, we change our focus to Gd. Unlike the itinerant magnetism in the 3d transition metals, the magnetism in Gd is dominated by the half-filled 4f shell with a total magnetic moment of $7.0 \mu_B$, which by intra-atomic exchange interaction induces a smaller moment of $0.55 \mu_B$ in the 5d6s valence band. Recently, it has been found that down to the picosecond timescale, the coupling is strong enough to cause a simultaneous demagnetization of the itinerant 5d6s moments and the localized 4f moments. Evidence has been provided for Gd (refs 15, 17 and Wietstruk *et al.*, submitted), as well as Gd/Fe multilayers²⁶. Supported by these findings, we assign the total (4f + 5d6s) moments to μ_{at} in equation (1), while assuming that the driving spin-flip processes are entirely dominated by Elliott–Yafet processes in the 5d6s valence band. This scenario is shown in Fig. 1d,g. Using $\mu_{at} = 7.55 \mu_B$ and $T_C = 297$ K yields for Gd a figure of merit, T_C/μ_{at} , that is a factor of 25 smaller than that of Ni and Co. This very low T_C/μ_{at} would readily predict type II dynamics for Gd, if it would have a similar a_{sf} as Ni and Co.

In agreement with the prediction of type II dynamics, recent experiments have indeed shown such a two-step demagnetization process. High-resolution XMCD experiments (including low- α and femtosecond-slicing mode) were carried out on the $M_{4,5}$ -edge of Gd for 10-nm films on several substrates at 120–140 K, and using a fluence such that T_p reaches almost T_C after electron–phonon equilibration. An initial decrease by $\Delta m_1 \approx 25\%$ within $\tau_1 = 1.0 \pm 0.2$ ps, and a final demagnetization at $\tau_M = 40 \pm 10$ ps were observed^{15,17} (Wietstruk *et al.*, submitted). Using the M3TM, we fitted a_{sf} to match τ_M , τ_1 and Δm_1 simultaneously, and obtained $a_{sf} = 0.08 \pm 0.02$ (see Supplementary Information), that is, within a factor of two from Ni and Co.

To verify that a_{sf} of Ni, Co and Gd are of the same order of magnitude, we have calculated $\langle b^2 \rangle$ of Gd by the *ab initio* electron

theory (Table 1). In this case, ψ_k in equation (2) stands for the 5d, 6s and 6p states, which are excited by the laser pulse, whereas the 4f states are assumed to be unaffected by the laser beam and are treated as core states²⁷. Table 1 shows that also for Gd, the calculated value of a_{sf} fits with the one deduced from the experiments. Moreover, in the last two columns the demagnetization times as measured are compared to predictions from our theory using *ab initio* results for $\langle b^2 \rangle$. The observation of an almost three orders of magnitude slower demagnetization for Gd is readily reproduced. In passing, we emphasize that for Gd, τ_M as predicted from our Elliott–Yafet theory, becomes approximately equal to rough estimates of the spin-lattice relaxation time of 48 ps (ref. 2). Therefore, unlike for Ni and Co, a significant contribution by spin-lattice relaxation cannot be ruled out for Gd.

All results on Ni, Co and Gd discussed so far are collected in Fig. 4. Representing the results this way shows that the behaviour of Ni and Co is actually quite close to the boundary between the two regimes. This would mean that Ni might be a material that can be driven to the type II regime at higher T_0 . The simulations shown in Fig. 4b indeed predict that carrying out a demagnetization study on Ni at 550 K, that is, just below T_C , should show such an anomalous behaviour.

After having satisfactorily rounded up the story for the elementary ferromagnets, we conjecture that for other materials the same classification will be useful as well, although the microscopic mechanisms may be richer, and no longer entirely captured by equation (1). Certainly, type I dynamics is shown by several 3d transition-metal alloys such as NiFe, CoPt₃ (see ref. 4 and references therein) and GdFeCo (ref. 28), as well as multilayers such as Fe/Gd (ref. 26) and Co/Pt (ref. 29). In contrast, type II behaviour has been reported for rare-earth/transition-metal alloys (TbFe; ref. 30), several oxides (such as CrO₂, refs 31, 32; Sr₂FeMoO₆, ref. 33; and La_{1-x}Sr_xMnO₃, refs 32, 34), chalcogenides (CoCr₂S₄, CuCr₂Se₄, ref. 34) and magnetic semiconductors (InMnAs, ref. 35). In many of these cases, two magnetic timescales have been assigned. On the basis of the present work, such assignments need to be carefully readdressed—although models intrinsically related to highly excited electrons, such as proposed for CrO₂ (ref. 31) and TbFe alloys³⁰, cannot be ruled out *a priori*. However, without intending to push our simple model too much for the ferrimagnetic TbFe case, the observation in Fig. 4c that experimental data of ref. 30 can be well reproduced by the M3TM (see also Supplementary Information), calls for more research in this direction. Further extensions of the M3TM might profit from recent conjectures. As an example, the factor $(1 - P)$ introduced by Müller *et al.* to account for the (large) spin polarization P of certain materials³² could be added as a prefactor in equation (1). Furthermore, possible consequences of recent claims that demagnetization may be accompanied by a shrinking of the valence band width⁷ will have to be thought over carefully.

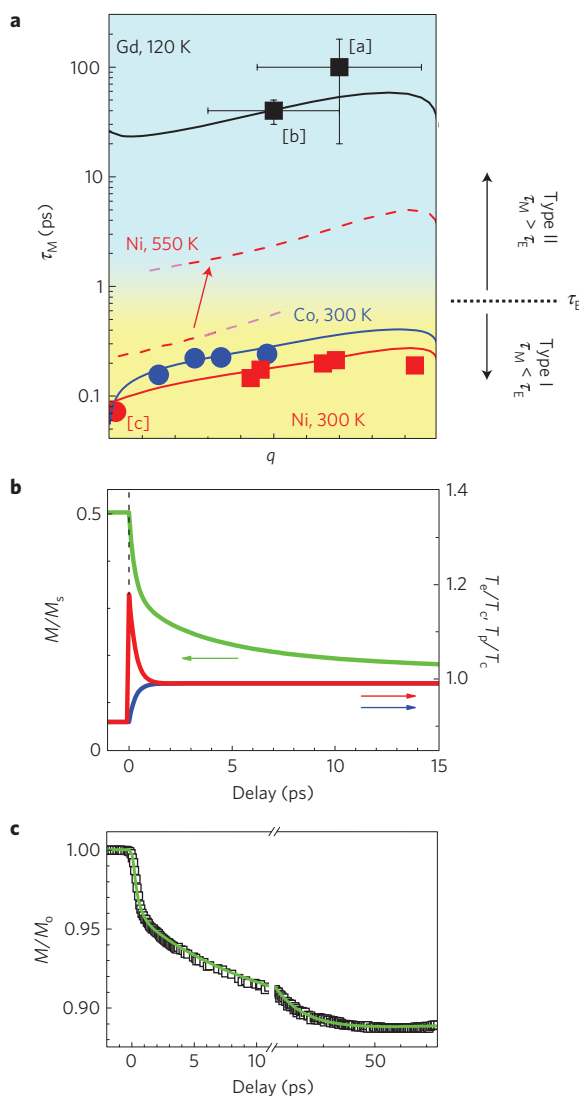


Figure 4 | Exploring the parameter space of type II dynamics. **a**, Overview of results, plotting calculated results (lines) and selected experimental data (symbols) for the demagnetization time τ_M as a function of laser fluence (magnetization quenching q). All simulations are for infinitesimally thin, free-standing films, and using $a_{sf} = 0.09, 0.150$ and 0.185 , for Gd, Co and Ni, respectively. Experimental data, as far as not from present work, are from: [a], ref. 1; [b], ref. 17 and Wietstruk *et al.* (submitted); [c], ref. 21. The vertical error bars are as reported in the cited references. The horizontal error bars are guides to the eye, emphasizing that for slow dynamics the quenching fraction depends strongly on heat diffusion. Nickel data at 550 K are a prediction, showing a transition from type I (single-step demagnetization) to type II (two-step demagnetization) as a function of laser fluence. **b**, Calculated $m(t)$ (green), $T_e(t)$ (red) and $T_p(t)$ (blue) for Ni at 550 K and a fluence corresponding to $q = 0.65$, showing the two-step behaviour characteristic for type II dynamics. **c**, Magnetization transient measured by TRMOKE on a $\text{Tb}_{35}\text{Fe}_{65}$ alloy (squares; data by Kim *et al.*³⁰), fitted by the M3TM (green line), clearly showing a type II behaviour.

The foregoing analysis shows that our M3TM quantitatively reproduces laser-induced demagnetization for a wide range of ferromagnets on equal footing. The large difference between the demagnetization timescales for the 3d transition metals such as Ni and Co, as well as the 4f rare-earth Gd can be explained by a simple figure of merit, T_C/μ_{at} . The only adjustable parameter, a_{sf} , is found to match well with *ab initio* estimates, and a complete picture emerges by assuming a thermalized electron gas. Thus,

after almost 20 years of research, it has become clear why both Vaterlaus¹ and Beaurepaire³ were right, even though the timescales for laser-induced loss of magnetization they found differed by three orders of magnitude.

Methods

Microscopic 3TM. Our approach to describe the magnetization dynamics in (multilayered) materials is based on a simplified model Hamiltonian⁹, describing (spinless) free electrons, representing phonons within the Einstein model (identical oscillators with energy E_p) and treating spin excitations using a mean-field Weiss model. For the sake of simplicity, we neglect the spin specific heat, and assume instantaneous thermalization of the electron gas. C_p is assumed to be independent of T , and we use $C_e = \gamma T_e$, where γ is a materials-dependent parameter. Thus, we derive (see Supplementary Information) a set of three coupled differential equations that completely specify the magnetization dynamics (note that the last equation is identical to equation (1)):

$$C_e[T_e] \frac{dT_e}{dt} = \nabla_z(\kappa \nabla_z T_e) + g_{ep}(T_p - T_e)$$

$$C_p \frac{dT_p}{dt} = g_{ep}(T_e - T_p) \quad (3)$$

$$\frac{dm}{dt} = Rm \frac{T_p}{T_C} \left(1 - m \coth\left(\frac{mT_C}{T_e}\right) \right)$$

where ∇_z denotes differentiation with respect to z , and κ is the (electronic) thermal conductivity and T_e , T_p and m are a function of z , the coordinate perpendicular to the film surface. Furthermore,

$$R = \frac{8a_{sf}g_{ep}k_B T_C^2 V_{at}}{(\mu_{at}/\mu_B)E_D^2}$$

where V_{at} is the atomic volume and k_B is the Boltzmann constant. Using a slightly more realistic phonon density of states according to the Debye model, we derived $E_p^2 = E_D^2/2$ (with E_D the Debye energy) as the most appropriate choice for E_p (Supplementary Information). Rather than modelling a realistic source (heating) term, we assume instantaneous heating of the electron system to a temperature profile $T_e(z, 0) = \Delta T_e(0, 0) \exp(-z/\lambda)$, where λ is the optical penetration depth. Throughout our article, we mostly treat the simple (intrinsic) case of ultrathin and thermally isolated films, in which case the z dependence can be neglected. For quantitative comparison to experiments, we use a more realistic extended (multilayer) film approach, using a finite λ , and calculating the magneto-optical signal according to the same exponential dependence as the laser excitation.

In our analysis, we use literature values for κ , room temperature specific heat ($C_p + \gamma \cdot 300$ K), E_D , T_C , μ_{at} and V_{at} (see Supplementary Information). The only fitting parameters to adjust to experimental TRMOKE transients are g_{ep} (determining the cooling down of the electron gas), a_{sf} (determining the initial steepness of the demagnetization transient) and the ratio C_p/γ (determining the magnitude of the initial peak relative to the final demagnetization). Furthermore, we fitted an extra instantaneous state-filling contribution²¹, and heat dissipation into the substrate is treated in a simplified way (see Supplementary Information for more details).

Experimental set-up and sample preparation. The detailed experimental set-up for the TRMOKE measurements in the high-fluence regime has been described elsewhere^{12,36}. Briefly, a two-colour pump-probe experiment is applied, where the pump pulses are generated by a Ti:sapphire multipass amplifier operating at a repetition rate of 1 kHz and a central wavelength of 800 nm, and the probe pulses are generated by frequency doubling. Optimization of the amplifier's internal compressor and prism group-velocity dispersion compensation lead to a full-width at half-maximum of 50 fs for both the pump and the probe pulse. Experiments were carried out in the longitudinal Kerr configuration. The pump pulse (s-polarized) is at normal incidence and the probe pulse (s-polarized) impinges under an angle of 45° on the sample surface. An active beam stabilization (BeamLock 4D, developed and manufactured by TEM Messtechnik) is used to ensure the spatial beam overlap on the sample and to avoid pointing drift during the measurements. For detection purposes, we use a balanced optical bridge with subsequent lock-in filtering. (To achieve further noise filtering, a 2σ-acceptance window is implemented in the data analysis program³⁷.) The Kerr rotation is obtained by subtracting TRMOKE signals for the opposite in-plane saturation fields.

The samples under investigation are thin polycrystalline ferromagnetic films: a 15-nm-thick cobalt film deposited on MgO by dc-sputtering and a 15-nm-thick Ni film deposited on Si by electron-beam evaporation. The Ni film is capped with 3 nm of titanium and a further layer of 3 nm titanium acts as an adhesion promoter between the Ni and the substrate.

Ab initio calculations of spin-mixing. The calculations of $\langle b^2 \rangle$ are carried out by the *ab initio* density functional electron theory in the local spin-density approximation, using a correlation part from ref. 38, an exchange part from ref. 39 and by the tight-binding linear-muffin-tin-orbital method⁴⁰ with the spin-orbit coupling implemented according to ref. 41. As the laser pulse heats up the system more or less immediately, we assume that after the pulse the excited electrons occupy electronic states of the effective zero-temperature ground-state potential that were unoccupied before the pulse.

In general, a calculation of the full spin-flip probability a_{sf} requires the determination of matrix elements for the transitions. However, under simplifying assumptions, a_{sf} may be represented as $a_{sf} = p\langle b^2 \rangle$, where handwaving arguments^{18,19,24} show that p should be of the order of unity (Fabian and Das Sarma²⁴ deduced $p = 4$, for example). Both Elliott and Yafet have pointed out that the prefactor p is not universal, but depends on the material and may vary roughly between 1 and 10, which is the uncertainty we adopt in the present work (see the range in Table 1).

Received 30 March 2009; accepted 3 November 2009;
published online 13 December 2009

References

- Vaterlaus, A., Beutler, T. & Meier, F. Spin-lattice relaxation time of ferromagnetic gadolinium determined with time-resolved spin-polarized photoemission. *Phys. Rev. Lett.* **67**, 3314–3317 (1991).
- Hübner, W. & Bennemann, K. H. Simple theory for spin-lattice relaxation in metallic rare-earth ferromagnets. *Phys. Rev. B* **53**, 3422–3427 (1996).
- Beaurepaire, E., Merle, J.-C., Daunois, A. & Bigot, J.-Y. Ultrafast spin dynamics in ferromagnetic nickel. *Phys. Rev. Lett.* **76**, 4250–4253 (1996).
- Koopmans, B. *Handbook of Magnetism and Advanced Magnetic Materials* Vol. 3, 1589–1613 (Wiley, 2007).
- Scholl, A., Baumgarten, L., Jacquemin, R. & Eberhardt, W. Ultrafast spin dynamics of ferromagnetic thin films observed by fs spin-resolved two-photon photoemission. *Phys. Rev. Lett.* **79**, 5146–5149 (1997).
- Rhie, H. S., Dürr, H. A. & Eberhardt, W. Femtosecond electron and spin dynamics in Ni/W(110) films. *Phys. Rev. Lett.* **90**, 247201 (2003).
- Stamm, C. *et al.* Femtosecond modification of electron localization and transfer of angular momentum in nickel. *Nature Mater.* **6**, 740–743 (2007).
- Zhang, G. P. & Hübner, W. Laser-induced ultrafast demagnetization in ferromagnetic metals. *Phys. Rev. Lett.* **85**, 3025–3028 (2000).
- Koopmans, B., Ruigrok, J. J. M., Dalla Longa, F. & de Jonge, W. J. M. Unifying ultrafast magnetization dynamics. *Phys. Rev. Lett.* **95**, 267207 (2005).
- Djordjevic, M. & Münzenberg, M. Connecting the timescales in picosecond remagnetization experiments. *Phys. Rev. B* **75**, 012404 (2007).
- Kazantseva, N. *et al.* Towards multiscale modelling of magnetic materials: Simulations of FePt. *Phys. Rev. B* **77**, 184428 (2008).
- Cinchetti, M. *et al.* Spin-flip processes and ultrafast magnetization dynamics in Co: Unifying the microscopic and macroscopic view of femtosecond magnetism. *Phys. Rev. Lett.* **97**, 177201 (2006).
- Melnikov, A. *et al.* Coherent optical phonons and parametrically coupled magnons induced by femtosecond laser excitation of the Gd(0001) surface. *Phys. Rev. Lett.* **91**, 227403 (2003).
- Loukakos, P. A. *et al.* Dynamics of the self-energy of the Gd(0001) surface state probed by femtosecond photoemission spectroscopy. *Phys. Rev. Lett.* **98**, 097401 (2007).
- Melnikov, A. *et al.* Nonequilibrium magnetization dynamics of gadolinium studied by magnetic linear dichroism in time-resolved 4f core-level photoemission. *Phys. Rev. Lett.* **100**, 107202 (2008).
- Bovensiepen, U. Coherent and incoherent excitations of the Gd(0001) surface on ultrafast timescales. *J. Phys. Condens. Matter.* **19**, 083201 (2007).
- Wietstruk, M. *et al.* *International Conference on Ultrafast Surface Dynamics* 6, Kloster Banz, Germany, 20–25 July (2008).
- Elliott, R. J. Theory of the effect of spin-orbit coupling on magnetic resonance in some semiconductors. *Phys. Rev.* **96**, 266–279 (1954).
- Yafet, Y. in *Solid State Physics* Vol. 14 (eds Seitz, F. & Turnbull, D.) (Academic, 1963).
- Kazantseva, N., Nowak, U., Chantrell, R. W., Hohlfield, J. & Rebei, A. Slow recovery of the magnetization after a sub-picosecond heat pulse. *Europhys. Lett.* **81**, 27004 (2008).
- Dalla Longa, F., Kohlhepp, J. T., de Jonge, W. J. M. & Koopmans, B. Influence of photon angular momentum on ultrafast demagnetization in nickel. *Phys. Rev. B* **75**, 224431 (2007).
- van Kampen, M., Kohlhepp, J. T., de Jonge, W. J. M., Koopmans, B. & Coehoorn, R. Sub-picosecond electron and phonon dynamics in nickel. *J. Phys. Condens. Matter.* **17**, 6823–6834 (2005).
- Beneu, F. & Monod, P. The Elliott relation in pure metals. *Phys. Rev. B* **18**, 2422–2425 (1978).
- Fabian, J. & Das Sarma, S. Spin relaxation of conduction electrons in polyvalent metals: Theory and a realistic calculation. *Phys. Rev. Lett.* **81**, 5624–5627 (1998).
- Pickel, M. *et al.* Spin-orbit hybridization points in the face-centered-cubic cobalt band structure. *Phys. Rev. Lett.* **101**, 066402 (2008).
- Bartelt, A. F. *et al.* Element-specific spin and orbital momentum dynamics of Fe/Gd multilayers. *Appl. Phys. Lett.* **90**, 162503 (2007).
- Hummeler, K. & Fähnle, M. Full-potential linear-muffin-tin-orbital calculations of the magnetic properties of rare-earth-transition-metal intermetallics. 1. Description of the formalism and application to the series RCo(5) (R = rare-earth atom). *Phys. Rev. B* **53**, 3272–3289 (1996).
- Stanciu, C. D. *et al.* Ultrafast spin dynamics across compensation points in ferrimagnetic GdFeCo: The role of angular momentum compensation. *Phys. Rev. B* **73**, 220402(R) (2006).
- Malinowski, G. *et al.* Control of speed and efficiency of ultrafast demagnetization by direct transfer of spin angular momentum. *Nature Phys.* **4**, 855–858 (2008).
- Kim, J. W., Lee, K.-D., Jeong, J.-W. & Shin, S.-C. Ultrafast spin demagnetization by nonthermal electrons of TbFe alloy film. *Appl. Phys. Lett.* **94**, 192506 (2009).
- Zhang, Q., Nurmikko, A. V., Miao, G. X., Xiao, G. & Gupta, A. Ultrafast spin-dynamics in half-metallic CrO₂ thin films. *Phys. Rev. B* **74**, 064414 (2006).
- Müller, G. *et al.* Spin polarization in half-metals probed by femtosecond spin excitation. *Nature Mater.* **8**, 56–61 (2009).
- Kise, T. *et al.* Ultrafast spin dynamics and critical behaviour in half-metallic ferromagnet: Sr₂FeMoO₆. *Phys. Rev. Lett.* **85**, 1986–1989 (2000).
- Ogasawara, T. *et al.* General features of photoinduced spin dynamics in ferromagnetic and ferrimagnetic compounds. *Phys. Rev. Lett.* **94**, 087202 (2005).
- Wang, J. *et al.* Ultrafast quenching of ferromagnetism in InMnAs induced by intense laser irradiation. *Phys. Rev. Lett.* **95**, 167401 (2005).
- Roth, T. *et al.* Dynamics of the coercivity in ultrafast pump-probe experiments. *J. Phys. D* **41**, 164001 (2008).
- Anderson, E. H. K., Sewall, S. L., Cooney, R. R. & Kambhampati, P. Noise analysis and noise reduction methods in kilohertz pump-probe experiments. *Rev. Sci. Instrum.* **78**, 073101 (2007).
- Perdew, J. P. & Wang, Y. Accurate and simple analytic representation of the electron-gas correlation-energy. *Phys. Rev. B* **45**, 13244–13249 (1992).
- Perdew, J. P. & Yue, W. Accurate and simple density functional for the electronic exchange energy—generalized gradient approximation. *Phys. Rev. B* **33**, 8800–8802 (1986).
- Andersen, O. K. & Jepsen, O. Explicit, first-principles tight-binding theory. *Phys. Rev. Lett.* **53**, 2571–2574 (1984).
- Ederer, C., Komelj, M., Fähnle, M. & Schütz, G. Theory of induced magnetic moments and X-ray magnetic circular dichroism in Co–Pt multilayers. *Phys. Rev. B* **66**, 094413 (2002).

Acknowledgements

We acknowledge U. Bovensiepen for highly enlightening discussions, which significantly contributed to the insight that led to the present work. We are indebted to D. Steil (TU Kaiserslautern) who participated in the TRMOKE measurements. M. Jourdan (Universität Mainz) and C. Döring (TU Kaiserslautern) are acknowledged for sample preparation. We thank the DFG SPP 1133 and the GRK 792 ‘Nonlinear Optics and Ultrafast Processes’, as well as the EU network Ultraswitch for financial support.

Author contributions

The M3TM was developed by B.K. and F.D.L.; experimental work was carried out by T.R. and F.D.L.; data analysis and simulations were done by B.K., T.R., G.M. and M.C.; D.S. and M.F. carried out *ab initio* calculations and provided theory input, and project planning was taken care of by B.K., M.C., M.A. and M.F. B.K. wrote the core of the manuscript, and all authors contributed to certain parts of it.

Additional information

The authors declare no competing financial interests. Supplementary information accompanies this paper on www.nature.com/naturematerials. Reprints and permissions information is available online at <http://npng.nature.com/reprintsandpermissions>. Correspondence and requests for materials should be addressed to B.K.